Ocean Modelling 183 (2023) 102182

Contents lists available at ScienceDirect

Ocean Modelling

journal homepage: www.elsevier.com/locate/ocemod

Spectral wave modeling of bimodal sea states at laboratory and coastal scales

Antoine Villefer [a,b,*], Michel Benoit [a,b], Damien Violeau [a,b], Maria Teles [a]

[a] EDF R&D Laboratoire National d'Hydraulique et Environement (LNHE), 6 quai Watier, Chatou, 78400, France
[b] LHSV, EDF R&D, École des Ponts, 6 quai Watier, Chatou, 78400, France

ARTICLE INFO

Keywords:
Bimodal sea states
Wind waves
Swell
Wind-wave tunnel
Spectral wave model

ABSTRACT

A downshift of the wind wave peak frequency was observed in a wind wave tunnel when irregular long paddle-waves (i.e. generated mechanically with a plane wave-maker) are added in the sea state. The 3rd generation spectral wave model, TOMAWAC, is used to assess the extent at which this peak frequency downshift can take place at prototype scale in bimodal sea-state conditions involving swell and wind wave systems. Several parameterizations of the modeled physical processes are selected to numerically reproduce the laboratory experiments in the first place. Then, the model performances are further inquired in reproducing coastal observations during a specific event combining a wind wave and a swell system. Overall, a good agreement is obtained between the simulations and the observations both at laboratory and coastal scale. In particular, a set of parameterizations combining one of the latest developments in spectral wave models for the whitecapping dissipation and the nonlinear 4-wave interactions reveals high performances in reproducing the observations. Lastly, based on the performances of this latter set of parameterizations, a generic numerical domain with typical coastal scale dimensions is created to inquire the occurrence of the downshift at prototype scale. This last study reveals a wind wave peak period shift from 5 s without swell to more than 6.5 s with a 2 m high swell.

1. Introduction

Sea states combining several wave systems, such as swell and wind waves, are very common both in open oceans and in coastal areas (Thompson et al., 2018; Mason et al., 2008). Although the occurrence of these complex sea states has been addressed several times in the literature, it is not quite settled whether the wind waves are generated the same way with or without a background swell. The purpose of this paper is to evaluate 3rd generation (hereafter denoted 3G) wave models performances for bimodal sea states modeling, given recent improvements in wind wave generation parameterizations. Then, such a model is further used to investigate the physics behind the combinations of both wave systems.

With the purpose to study wind wave growth in the presence of swell, a preliminary approach consists in studying the generation of short wind waves in the presence of a longer wave system in the well controlled conditions of a wind wave tank. Such facilities allow the combination of both wave systems generated using an air blower and a mechanical paddle-wave-maker, respectively Mitsuyasu (1966), Phillips and Banner (1974), Donelan (1987) and Villefer et al. (2021). Yet, the long paddle-waves generated in wind wave tanks are significantly different from ocean swell in terms of wave age $\xi = c_p/U_{10}$, with c_p the peak phase celerity and U_{10} the wind velocity at 10 m above the mean water level (MWL). Respective wave ages are larger than 1 for typical ocean swell and generally lower than 0.5 for paddle-waves in wind wave tanks to avoid surface tension effects. Therefore, the different wave systems generated in a wind wave tank should be considered as different components of the wind sea (with lower and higher peak frequencies), rather than real swell and wind sea. Hereafter, for readability reasons, short wind-generated waves are denoted "wind waves" and long mechanically-generated waves are denoted "paddle-waves".

Donelan's (1987) wind wave tank experiments revealed a reduction of the wind-sea variance by a factor of about 2.5 in the presence of following monochromatic paddle-waves. Replacing the monochromatic waves by JONSWAP-type paddle-waves, Villefer et al. (2021) showed that the wind wave peak frequency is shifted towards lower frequencies due to the background paddle-waves. However, the extension of these results for the study of wind wave growth over real ocean swell is complicated by the high steepness and the low wave age of the laboratory paddle-waves compared to open-ocean swell.

At prototype scale, a common approach to physically characterize such a bimodal sea state involves in-situ observations of its spatial development. Thus, the conditions for these observations must be in a coastal area where a wind is blowing steadily offshore (i.e. fetch-limited conditions) and opposing a swell directed inshore (Ardhuin et al., 2007; Hwang et al., 2011). These very specific conditions make the

* Corresponding author at: EDF R&D Laboratoire National d'Hydraulique et Environement (LNHE), 6 quai Watier, Chatou, 78400, France.
E-mail address: antoine.villefer@edf.fr (A. Villefer).

https://doi.org/10.1016/j.ocemod.2023.102182
Received 16 September 2022; Received in revised form 22 December 2022; Accepted 17 February 2023
Available online 25 February 2023

characterization of bimodal sea states rather difficult at natural scale. Some observations showed a modification of wind wave growth in the presence of swell (Donelan et al., 1997; Hwang et al., 2011; Vincent et al., 2019). According to Hwang et al. (2011), wind wave generation and development are enhanced with an opposing background swell. These observations lead to physical interpretations: swell is expected to modify the wind velocity profile (Donelan et al., 1997; Chen and Belcher, 2000), to increase the breaking of the wind sea (Phillips and Banner, 1974) and to alter the nonlinear 4-wave interactions (Masson, 1993). However, based on observations in the North Carolina continental shelf during the Shoaling Waves Experiment (SHOWEX), Ardhuin et al. (2007) showed that a moderate swell has no significant effect on the bulk parameters characterizing the wind sea.

Both the idealized laboratory conditions and the realistic in-situ observations are necessary to understand the processes at play when wind waves are generated over a preexisting swell. With the purpose to unify the different observations, our approach is based on the use of the 3G spectral wave model TOMAWAC (part of the TELEMAC-MASCARET hydro-informatic system) (Benoit et al., 1996) to upscale (Villefer et al., 2021) laboratory results to the coastal scale. The model is used to numerically reproduce first the laboratory experiments and then an event during the SHOWEX campaign. Taking advantage of the physical processes separation involved in wind wave generation, the laboratory experiments hindcast aims to assess the extent at which the observed spectral downshift can occur at prototype scale.

However, the accuracy of 3G wave models remains questionable for a simulation including more than one wave system as shown in latest developments in 3G wave models (Ardhuin et al., 2010; Gagnaire-Renou et al., 2010). While the integral parameters such as the significant wave height and representative periods can be well predicted for this kind of sea states, the frequency and directional distributions of the wave energy remain rather inaccurate. However, these distributions are of prime importance for applications such as the design of coastal protections or offshore structures.

Recent developments in wave models proved that improving the whitecapping dissipation modeling was necessary to better simulate the combination of swell and wind sea. This dissipation process is considered as the least understood part of the physics relevant to wave modeling by Cavaleri et al. (2007).

The first operational dissipation parameterization in 3G wave models was the one developed by Komen et al. (1984) loosely following Hasselmann (1974)'s work in which whitecaps act as a pressure pulse countering the rise of the sea surface. In the case of swell and wind wave combination, the main weakness of this parameterization is the use of an averaged wave steepness to determine the dissipation rate. Since swell and wind waves have a low and high steepness respectively, the presence of swell leads to anomalously high wind waves due to a lack of dissipation and vice-versa. Bidlot et al. (2007) partly corrected this issue by re-defining the averaged steepness used in the latter parameterization to increase the dissipation at higher frequencies (i.e. wind wave frequencies).

To further solve this issue, dissipation models using a local saturation spectrum rather than an integral wave steepness have been developed based on the work of Alves and Banner (2003). First, van der Westhuysen (2007) combined the advantages of a saturation model (van der Westhuysen et al., 2007) and a model based on the average wave steepness of the sea state (Komen et al., 1984). Secondly, Ardhuin et al. (2010) developed a new set of source/sink terms taking into account the breaking threshold approach with a saturation term, the dissipation of short waves by larger breakers and the swell dissipation over long distances.

Another improvement in the bimodal sea state modeling regards the nonlinear 4-wave interactions. An exact equation with Boltzmann-type integral describing these interactions has been proposed by Hasselmann (1962) and Zakharov (1968). Since then, a substantial work has been devoted to find a good balance between a computationally efficient and an accurate resolution of these interactions. Masson (1993) showed that nonlinear 4-wave interactions are involved in bimodal spectra evolution when the ratio of long-wave to short-wave frequencies is greater than 0.6. The standard Discrete Interaction Approximation (DIA) method, that triggered the outbreak of 3G wave models, is a computationally efficient method to estimate these interactions. However, it suffers from many shortcomings regarding the frequency and directional distribution of wave energy compared to exact methods (Benoit, 2005). According to Masson's work, a more accurate method to solve the nonlinear 4-wave interactions might be required for bimodal spectra simulations. Based on the Gaussian Quadrature Method (GQM) (Lavrenov, 2001), Gagnaire-Renou et al. (2010) developed an algorithm using numerical integration methods of high accuracy. In the following, this original method is used to assess wind wave growth in the presence of swell both at laboratory and coastal scales.

To compare the simulations with observations, an appropriate scaling is applied following Kitaigorodskii (1961). In the present study, wind wave growth is described in two manners both based on a spectral analysis of the sea states: on the one hand using the variance density spectrum $E(f,\theta,x,t)$ at a location x and a time t, where f and θ are the wave frequency and direction respectively, on the other hand using the fetch X, peak frequency f_p and the total variance of the free-surface elevation $m_0 = \overline{\eta^2}$. Those variables are made dimensionless using U_{10} and the acceleration due to gravity g:

$$X^* = \frac{Xg}{{U_{10}}^2} \tag{1a}$$

$$f_p^* = \frac{f_p U_{10}}{g} \tag{1b}$$

$$m_0^* = \frac{m_0 g^2}{{U_{10}}^4} \tag{1c}$$

In the present paper, Section 2 presents the laboratory experiments (see Villefer et al. (2021) for a more complete description) and the SHOWEX event (Ardhuin et al., 2007) against which TOMAWAC's hindcast performances are evaluated. Section 3 gives an overview of the physics at play in the wave model in order to introduce the different sets of parameterizations later used for the simulations. Then, after a description of the numerical characteristics, the results of the simulations at laboratory and at coastal scales are discussed in Sections 4 and 5, respectively. In light of the preceding discussion, a generic numerical domain is created to assess wind wave growth modifications in the presence of a following swell at coastal scale in Section 6. Section 7 summarizes the present findings and introduces recent 3G wave model developments that could further improve the simulation of bimodal sea state conditions.

2. Bimodal sea states data sets

This section introduces two bimodal sea state data sets, used to evaluate the performances of TOMAWAC, during the wave generation process, at laboratory and coastal scales, respectively. It is important to note that these data sets are not comparable since they differ in at least two ways:

- a short and a long wind wave systems are combined in the wind wave tank whereas wind waves and oceanic swell coexist at coastal scale,
- both wave systems have the same direction in the wind wave tank whereas they have nearly opposed directions at coastal scale.

The extension of the laboratory results (i.e. the peak frequency downshift phenomenon) at coastal scale is investigated in Section 6.

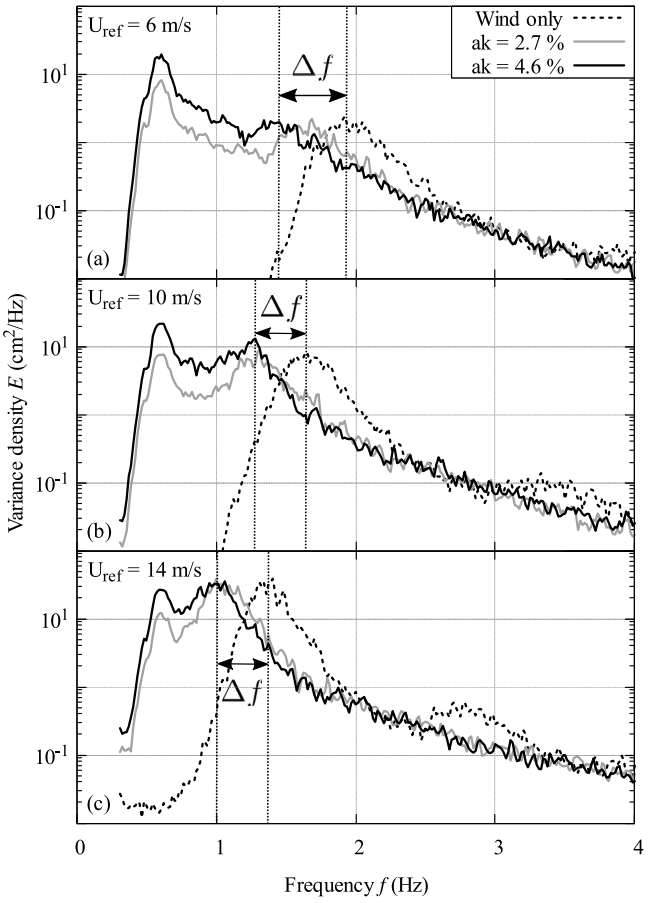

Fig. 1. Laboratory measurements of variance density spectra with and without irregular paddle-waves of steepness ak and peak frequency $f_p = 0.6$ Hz for three wind velocities U_{ref} at fetch 30 m (maximal fetch).

2.1. Experimental study in a wind wave tank

The first dataset consists in a series of experiments carried out in the controlled conditions of the Institut de Recherche sur les Phénomènes Hors-Equilibre (IRPHÉ)-Pythéas 40 m long wind wave tank in Marseilles, France. The use of such a facility permitted to study wind wave growth in the presence of following long paddle-waves. The facility and the results are described and discussed in Villefer et al. (2021). Twelve wave gauges distributed along the test section enabled to obtain the fetch-limited evolution of the wind waves with and without monochromatic or irregular (JONSWAP-type) paddle-waves.

For the present study, only the spectra depicting wind waves in the presence of irregular paddle-waves are considered using the wave gauge situated at the maximal fetch of 30 m. Fig. 1 introduces the 6 cases of interest for this study. The frequency wave spectra are considered for three wind-speed settings, $U_{\text{ref}} = 6$, 10 and 14 m/s, with and without paddle-waves. Here, U_{ref} is a reference wind speed measured by a sonic anemometer at 1 m above MWL. Two different values of paddle-wave steepness ak of 2.7 and 4.2%, with the wave amplitude $a = \sqrt{2m_0} = H_{m_0}/(2\sqrt{2})$ and the wavenumber $k = k_p$ (i.e. the peak wavenumber), are considered.

For each wind velocity in Fig. 1, the comparison between spectra with and without paddle-waves highlights the downshift of the wind wave frequency peak in the presence of paddle-waves. This downshift tends to increase with increasing paddle-wave steepness. By fitting the vertical profile of the horizontal wind velocity with a logarithmic profile method (see Monin and Obukhov (1954)), Villefer et al. (2021) found that the friction velocity at the air/sea interface $u_\star$ had a tendency to increase in the presence of a background following paddle-waves. This tendency can be retained as a first hypothesis to explain the above-mentioned downshift as a result of an increase of the momentum transfer from the wind to the waves with paddle-waves. The following numerical simulations are analyzed given these observed experimental features.

2.2. SHOWEX in-situ observations in North Carolina continental shelf

The second dataset considered for model's validation is an event that happened during the Shoaling Waves Experiment (SHOWEX) conducted in the North Carolina continental shelf (east coast of the USA) from August to December 1999. Six Datawell Directional Waverider (DDW) buoys (Ardhuin et al., 2003b,a) were deployed along a cross-shelf transect going from 5 to 80 km (X1 to X6) to the coastline (see Fig. 2) to obtain the wave spectra and bulk parameters. Three Air–Sea Interaction Spar (ASIS) buoys (Graber et al., 2000) permitted to obtain the wind properties and additional wave measurements (Bravo, Yankee and Romeo buoys in Fig. 2). Buoys and stations of the National Data Buoy Center (NDBC) and the U.S. Army Corps of Engineers (USACE) provided extra data about the oceanic and atmospheric conditions.

On 3rd November 1999, a 10 m/s wind (U_{10}), coming from the land (westerly wind, orange arrow in Fig. 2), was blowing steadily and uniformly over a time period of 5 h from 12:00 to 17:00 East-Coast Standard Time (EST). This led to wind wave generation close to idealized fetch-limited conditions with a wind directed at 10 to 30 degrees relative to the normal to the coast (i.e. slightly oblique wind). An additional southeasterly swell system (blue arrow in Fig. 2) with a peak period $T_p \simeq 10$ s and a significant wave height $H_s \simeq 1$ m was nearly opposed to the local wind. This event, first chosen by Ardhuin et al. (2007) to validate the spectral wave model WAVEWATCH III (WW3) (Tolman and Chalikov, 1996; The WAVEWATCH III (R) Development Group (WW3DG), 2019), provides rare observations of fetch-limited conditions, in the presence of a background swell, with a large set of wave sensors to assess wind wave growth with fetch.

The wave spectra calculated from the wave buoys measurements, for instance at Bravo in Fig. 2, depicted the evolution of two well-defined wave systems: the low frequency part with swell energy decreasing from offshore to the coast and the high frequency (HF) part with wind waves growing with fetch from X1 to X6. Looking at Bravo directional spectrum in Fig. 2, one can observe that the wind wave peak is not exactly aligned with the mean wind direction (orange dots): the main wind wave components are slightly deviated towards the alongshore direction (i.e. $\theta \simeq 160°$). This observation, within the framework of this particular event, received two different interpretations in the literature. On the one hand, it was associated to slanting-fetch conditions (i.e. the obliquity of the wind direction relative to the normal to the coast) and to wave refraction by Ardhuin et al. (2007). The turning of the wind wave peak due to slanting-fetch conditions is further described in Pettersson et al. (2010). It is interesting to remark that the wind wave peak mean direction simulated with WW3 in Ardhuin et al. (2010), including the wave dissipation model they developed, showed a 25° bias towards the alongshore direction. On the other hand, Zhang et al. (2009) associated the turning of the wind wave peak towards the alongshore direction to a wind stress angle deviated from the wind direction because of surface currents.

Following Ardhuin et al. (2007) in the case of a slanting fetch, the dimensionless fetch in the wind direction is defined extending Eq. (1a) as $X^* = Xg/(\cos\theta_w U_{10}^2)$, where θ_w is the wind direction with respect to the normal to the coast and X is the distance perpendicular to the coast. The idealized fetch-limited condition, the specific directional properties of the observed spectra and the comparison with WW3 results (Ardhuin et al., 2007, 2010) provide a valuable database to assess the performances of the present simulations.

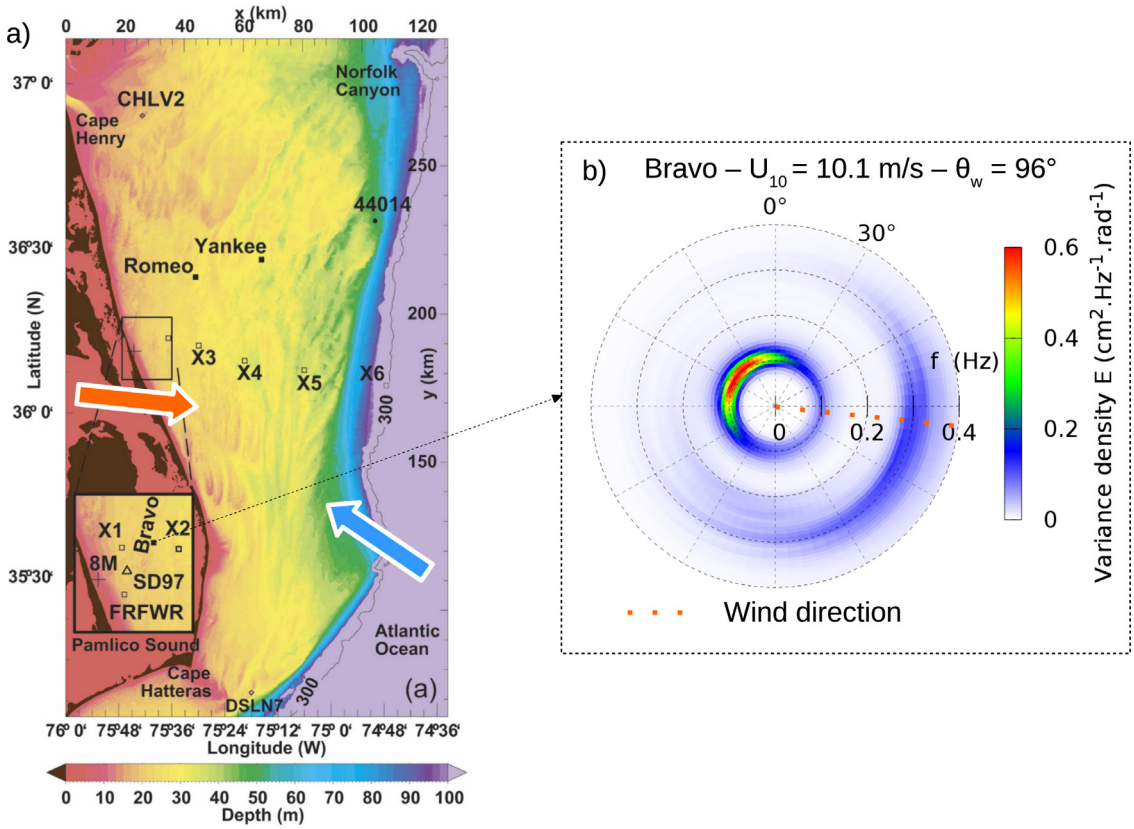

Fig. 2. (a) Bathymetry of the North Carolina shelf and locations of wave measurements during the SHOWEX campaign (1999) with a directional spectrum (b), obtained from the MLM and averaged from 12:00 to 17:00 (EST), at Bravo (ASIS-type buoy) illustrating the wind and wave conditions. The orange and the blue arrows depict wind and swell directions respectively. The left part of this picture was taken from Ardhuin et al. (2007).

3. Parameterization of the 3rd generation wave model

TOMAWAC is a 3G wave model (developed by EDF R&D) using unstructured spatial grid of the oceanic domain for solving the action balance equation (Benoit et al., 1996). To serve that purpose, the model simulates the evolution of the action density directional spectrum at each node of a spatial computational grid. The balance equation of wave action density is solved for each component (f_i, θ_j), with discrete frequencies f_i and directions θ_j. Each component of the action density spectrum changes in time and space under the effects of wave propagation and software-modeled physical processes. Based on the considerations in Ardhuin et al. (2007), the current is not taken into account in the present study. Thereby, only the evolution of the surface elevation variance spectrum $E(t, \boldsymbol{x}, f, \theta)$, at a location $\boldsymbol{x}$ and a time t, is considered using the following equation:

$$\frac{dE}{dt} = Q \tag{2}$$

The left hand size of the equation is the kinematic part and the right hand size gathers the contributions from the physical processes modeled using source and sink terms. Following Ardhuin et al. (2007), bottom friction dissipation is considered as negligible, here, so that Q is formulated as in deep water conditions:

$$Q = Q_{\text{in}} + Q_{\text{ds}} + Q_{\text{nl}} \tag{3}$$

corresponding to the processes of wind energy input Q_{in}, dissipation through white-capping Q_{ds} and nonlinear 4-wave interactions Q_{nl}. In the code, each process has several models and formulations that can be adapted to the particularities of the studied case. The different source/sink terms used in the course of this study are described below from the most to the less known physical mechanisms.

Q_{nl} is the only source term that has been formulated theoretically (Hasselmann, 1962; Zakharov, 1968) as a Boltzmann integral for resonant interactions between quadruplets of surface gravity waves, as said above. Among the methods that have been developed to calculate an approximated solution, the above-mentioned two methods are used here: DIA ($Q_{\text{nl}}^{\text{DIA}}$) and the more accurate, as well as computationally heavier, GQM ($Q_{\text{nl}}^{\text{GQM}}$). The GQM algorithm, as implemented in TOMAWAC with the default configuration, needs about 50 times the DIA CPU time to compute Q_{nl}.

The transfer of momentum from the wind to the sea Q_{in} is based on Miles' feedback mechanism and Janssen's quasi-linear theory for modeling the ocean/atmosphere interaction (Janssen, 1991, 2004), and denoted Q_{in}^{J}.

Lastly, the selected dissipation terms are van der Westhuysen (2007) term $Q_{\text{ds}}^{\text{VDW}}$, combining a saturation model (van der Westhuysen et al., 2007) and Komen et al. (1984)'s model, and Ardhuin et al. (2010) term $Q_{\text{ds}}^{\text{ST4}}$ (ST4 referring to WW3 nomenclature). This latter sink term is a combination of different dissipation terms formulated as $Q_{\text{ds}}^{\text{ST4}} = Q_{\text{sat}} + Q_{\text{bk,cu}} + Q_{\text{swell}} + Q_{\text{turb}}$. For the following simulations, the swell dissipation due to the resistance of the air Q_{swell} (Q_{out} in Ardhuin et al. (2010)) and the dissipation associated to surface turbulence Q_{turb} are considered as negligible. Particularly, Q_{swell} is not expected to have a significant effect on swell dissipation over the typical distances (150 km maximum) in the spatial domain considered here. Only the saturation term Q_{sat} and breaking cumulative term $Q_{\text{bk,cu}}$ (i.e. the dissipation of short waves by long breaking waves) are considered. The modification of Q_{in}^{J} and $Q_{\text{nl}}^{\text{DIA}}$ parameterizations described in Ardhuin et al. (2010) dissipation terms are included when $Q_{\text{ds}}^{\text{ST4}}$ is activated. Regarding Q_{in}^{J}, it consists in the inclusion of a sheltering effect, accounting for the effect of a background swell on the wind wave generation, by adapting the calculation of the friction velocity, somewhat like Chen and Belcher (2000) suggested. Amongst the parameterizations developed for $Q_{\text{ds}}^{\text{ST4}}$, we chose to use the T471f (The WAVEWATCH III (R) Development Group (WW3DG), 2019) which corresponds to the one used in WW3

at global scale adapted to Climate Forecast System Reanalysis (CFSR) wind files.

To reproduce both laboratory and in-situ SHOWEX observations, different sets of parameterizations for the source/sink terms are compared:

- VDW: $Q^{\mathrm{VDW}} = Q^{\mathrm{J}}_{\mathrm{in}} + Q^{\mathrm{VDW}}_{\mathrm{ds}} + Q^{\mathrm{DIA}}_{\mathrm{nl}}$, associated to blue color in figures of results,
- ST4: $Q^{\mathrm{ST4}} = Q^{\mathrm{J}}_{\mathrm{in}} + Q^{\mathrm{ST4}}_{\mathrm{ds}} + Q^{\mathrm{DIA}}_{\mathrm{nl}}$, associated to orange color,
- ST4 + GQM: $Q^{\mathrm{ST4+GQM}} = Q^{\mathrm{J}}_{\mathrm{in}} + Q^{\mathrm{VDW}}_{\mathrm{ds}} + Q^{\mathrm{GQM}}_{\mathrm{nl}}$, associated to red color.

These parameterizations will be compared with observations associated to gray scale colors.

4. Hindcast of laboratory experiments

4.1. Numerical specifications

A first series of simulations of the wind wave tunnel experiments led to some adjustments of the source/sink terms parameterizations. First, the wave growth limiter is deactivated. This limiter is generally used to guarantee the numerical stability of the calculation which, in our case, appears to be unnecessary with a small time step of 0.1 s. Secondly in $Q^{\mathrm{J}}_{\mathrm{in}}$, the friction velocity at the air/sea interface, for each wind speed U_{ref}, is forced to be constant and equal to the laboratory measured one in the "wind only" case, for simulations with and without paddle-waves. Without this forcing, the model tends to overestimate the friction velocity. In addition, the deep water approximation is adopted since it was shown by Villefer et al. (2021) that the dissipation due to bottom friction is relatively low.

Lastly, since the spectral wave model is not meant for the simulation of strictly unidirectional waves, the laboratory paddle-waves are modeled with a very narrow directional energy distribution:

$$E(f,\theta) = \frac{E(f)}{\Delta}\ \cos^{20}(\theta - \theta_0) \tag{4}$$

with $\theta \in [\theta_0 - \pi/2, \theta_0 + \pi/2]$ and Δ is a normalization factor to ensure that the integral of the angular spreading function over $[-\pi, \pi]$ is equal to 1. It was further verified that the following results with this representation of paddle-waves are not sensitive to the directional discretization. Yet, such a definition might change the nonlinear interactions between both wave systems that occurred in the wind wave tank. Therefore, the following results must be analyzed in light of the present directional definition of the paddle-wave system.

4.2. Results

Hindcasts of laboratory measurements (i.e. without any kinematic similarity) are not common in the literature. Booij et al. (2001) and Holthuijsen et al. (2000) made an attempt to simulate (Donelan, 1987) laboratory observations with the SWAN model (Booij et al., 1999). They showed significant limitations of 3G wave models to simulate wind wave generation and dissipation processes at laboratory scale. Indeed, wave models are exclusively parameterized for wave hindcasting or forecasting at global, regional or coastal scales. However, as Shemer (2019) showed, wave generation in wind wave tunnels is, to a great extent, comparable to in situ wind wave growth. Thus, using the advantages of the well-controlled laboratory environment can be a powerful way to validate 3G wave models.

Since the paddle-waves and the wind had the same direction in the tank, we focus on 1D (omnidirectional) wave spectra in this case. Fig. 3 depicts the observed spectra at a fetch 30 m by comparisons with the simulated ones. Columns and rows separate the different values of the steepness ak of irregular paddle-waves and the different wind speeds, respectively.

Overall, the simulations are in good agreement with the observed spectra in the presence of a JONSWAP-type paddle-waves. On the other hand, in "wind only" conditions, the spectral wind wave peak is underestimated in terms of energy and peak frequency. Booij et al. (2001) and Holthuijsen et al. (2000) raised a similar issue when simulating wind-wave growth from laboratory observations with SWAN. The most interesting point to highlight might be that, in the simulations, the various model variations seem to reproduce a wind wave peak frequency downshift in the presence of background long-waves. This numerically simulated downshift is however less pronounced than in the experiment.

It can be noted that the energy levels of the HF tail are overestimated in the simulations with $U_{\mathrm{ref}} = 10$ and 14 m/s (colored lines in Fig. 3.b,c,e and f) even if the variance density decrease rate at HF is consistent with the observations (grey scale). For those wind speeds, there is an increasing difference between the simulations and the observations from the wind wave peak to higher frequencies. It shows a lack of accuracy of the simulations in reproducing the well-known overshoot behavior (Barnett and Sutherland, 1968) associated to wind wave growth. At lower wind speed (Fig. 3.a and d), this overshoot is less pronounced and the HF tails seem rather well reproduced by the simulations including the long-waves. But it is not the case for the wind wave peak (colored dotted lines) which is underestimated in all panels. Overall, the simulation of an accurate energy level for both the wind wave peak and the HF tail seems to be a barrier when using 3G wave models at such small scale.

The different models described in Section 3 show different levels of performances in reproducing the observed spectra. First, the VDW set is the only parameterization depicting a slight underestimation of the low-frequency wave energy at the highest wind-speed. This is due to the limitation of Komen et al. (1984)'s parameterization partly included in VDW. At higher frequencies, VDW generally underestimates the energy of the wind wave peak with and without the long-waves. Such a behavior reveals an over dissipation of the wind-sea system in $Q^{\mathrm{VDW}}_{\mathrm{ds}}$. Regarding the "wind only" case, VDW simulates a wind wave peak frequency that tends to be shifted toward low frequencies by comparison with the observations.

At the largest wind speed $U_{\mathrm{ref}} = 14$ m/s, all the models tend to have an excessively energetic wind wave peak in the cases with long-waves and an excessively low wind wave peak frequency in "wind only" conditions. As highlighted in Villefer et al. (2021), the limitation of the techniques to measure the wind velocity profile could lead to the calculation of an excessive value of the friction velocity. Since the friction velocity forcing is taken from the experimental value, the wind wave peak energy and frequency can be expected to be respectively over- and under-estimated at higher wind speeds.

ST4 parameterization seems to better estimate the wind wave peak energy than VDW both with and without long waves, but still depicts a largely downshifted peak frequency for the "wind only" case. With a more accurate resolution for the 4-wave interactions with GQM, the simulations in "wind only" conditions give a better compromise in terms of energy level and peak frequency. The differences between ST4 with DIA and ST4 with GQM is well illustrated in the simulations with long-waves in Fig. 3.a and d. The red spectra (GQM) depict a slightly narrower wind wave peak than the orange spectra (DIA). Simulating narrower spectra is a well known property when improving the accuracy of the method for solving the 4-wave interactions (Benoit, 2005). Finally, considering the simulations with and without long-waves, ST4 + GQM might be the parameterization showing the best overall performances in reproducing the bimodal spectra observed in Marseilles' wind wave tank.

Fig. 4 is obtained by separating the wind waves from the paddle-waves using a decomposition of the sea state into two JONSWAP spectra fitted using a method presented in Villefer et al. (2021). It tempers the agreement between the simulated and the observed wind wave peak energy illustrated in Fig. 3. In Fig. 4.a, the 3G wave model overestimates the wind wave energy at all fetches with an exception at maximal fetch. Nevertheless, the simulated wind wave energy variations with fetch show a slope similar to Kahma and Calkoen (1992)

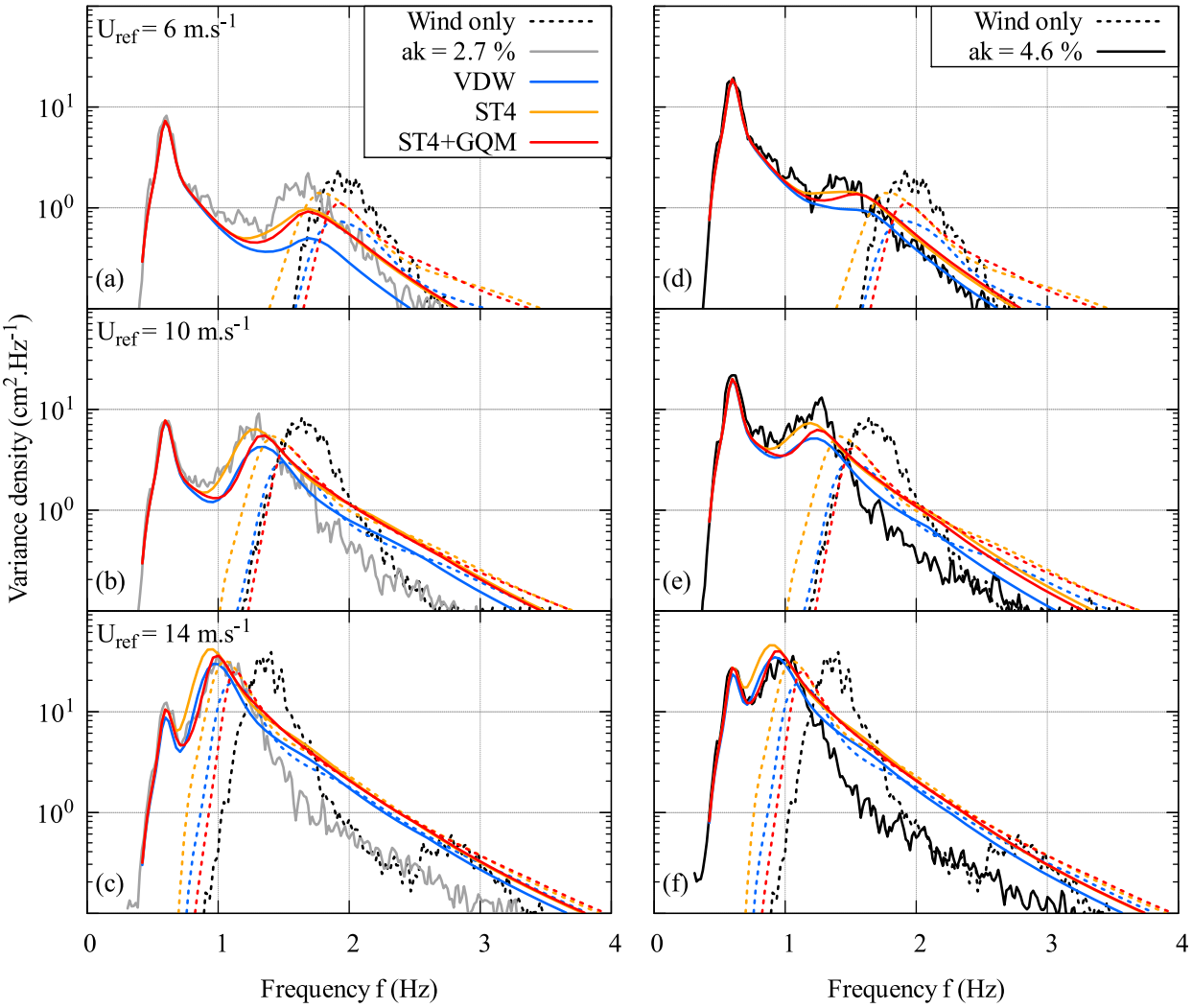

Fig. 3. Variance density spectra with and without irregular paddle-waves of steepness ak and peak frequency $f_p = 0.6$ Hz for several wind speeds (on rows) at a fetch of 30 m. Color lines (blue, orange and red) correspond to simulations with different sets of source/sink terms and black and gray lines refer to the observations.

formula and close to the observations. Regarding the simulated wind waves peak frequency variations with fetch, the model reproduces rather well the observed bimodal sea states in terms of magnitude and slope. However, the simulated variation of the wind wave peak frequency without paddle-waves (dotted lines in Fig. 4.b), clearly different from the corresponding observations (black squares), is similar to the observations with paddle-waves (black circles).

This latter issue, also observed in Fig. 3, is linked to the difficult question of triggering wind wave growth in 3G wave models. The wind wave growth initialization commonly used following Cavaleri and Malanotte Rizzoli (1981) was not adapted for wave simulation at laboratory scale in our case (not shown). Thus, we triggered wind wave growth by using the measured wind wave spectrum at a fetch 5 m as an input boundary condition in our simulations.

A difference is observed between the horizontal location of the HF peak of colored plain-line spectra and the corresponding peak of dotted-line spectra in Fig. 3, especially at high wind speed. This difference is observed, once again, in Fig. 4.b between the dashed and plain color lines. Hence, the downshift of the wind wave peak in the presence of long-waves, first observed during the laboratory experiments (Villefer et al., 2021), is observed once again in the simulations to a smaller extent. To further characterize this phenomenon, Fig. 5 illustrates the differences between its observations in laboratory (black dots) and their simulations (colored dots).

In laboratory, the downshift does not result in a modification of the wind wave energy. Hence, it implies a reduction of the wind wave steepness. This was illustrated, in a figure similar to Fig. 5 in Villefer et al. (2021), by the distance to Toba's law (Toba, 1997). Wind waves' steepness increases when the points overtake Toba's law from above. According to Fig. 5, at medium and high wind speed, the points are more gathered in the simulations than in the observations. Particularly, the most pronounced differences are in "wind only" conditions with the points corresponding to observed wind waves located above Toba's law contrary to the simulations. Thus, the model fails to reproduce the high steepness of the wind waves in "wind only" conditions.

For each wind speed and for all the parameterizations, the simulations exhibit a clear tendency to be horizontally distributed. The width of the distribution increases when the wind speed decreases, in agreement with the observations. The horizontal distribution shows that the wave models simulate wind waves with the same energy but a different peak frequency whether they are generated with or in absence of paddle-waves. Although, in "wind only" conditions, simulated wind waves are less steep than in laboratory, the simulations succeed in reproducing the wind wave frequency downshift happening when long-waves are added to the sea state.

In Villefer et al. (2021), the increase of the wind wave friction velocity in the presence of long waves was considered as a possible factor to explain the downshift. According to the simulations in which

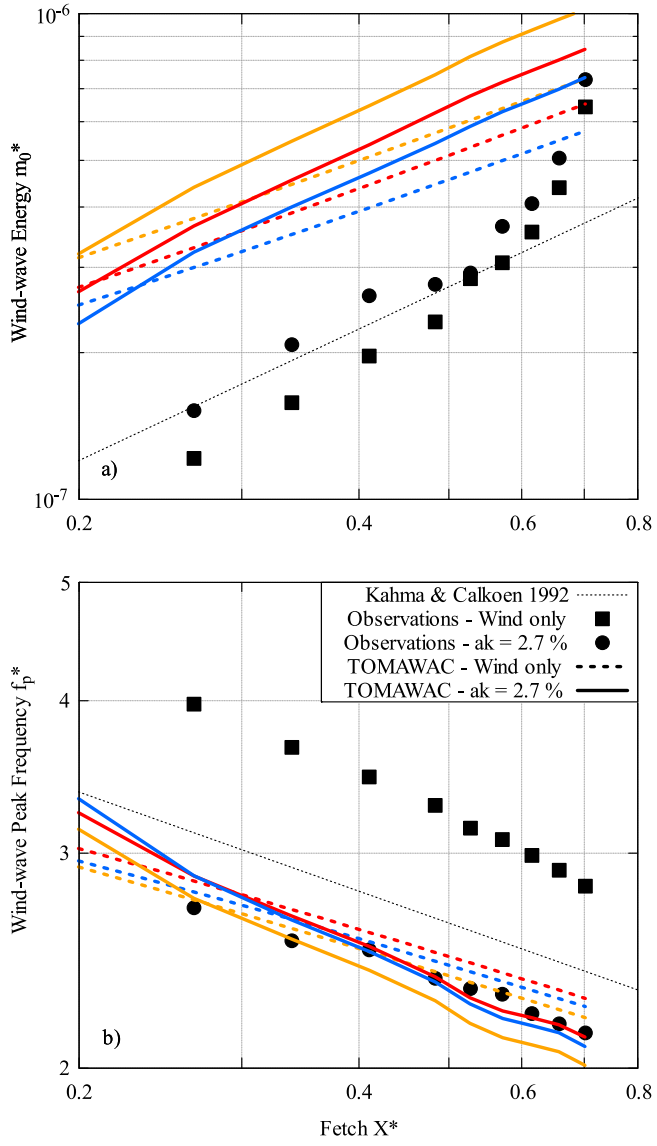

Fig. 4. Variations of the observed and simulated wind wave dimensionless energy (a) and peak frequency (b) with dimensionless fetch compared to Kahma and Calkoen (1992)'s empirical law for a wind speed U_{ref} = 14 m/s and irregular paddle-waves with ak = 2.7%. TOMAWAC's parameterizations are differentiated using colors: VDW in blue, ST4 in orange and ST4 + GQM in red. The black points refer to the observations.

the friction velocity is kept constant with and without long waves, this factor is proved not to be the only one explaining the downshift.

Overall, the simulations are in rather good agreement with the observed frequency spectra in cases including paddle-waves. Therefore, the narrow energy directional distribution selected to model the unidirectional paddle-waves does not seem to disturb the nonlinear interactions between both wave systems. The general underestimation of the wind wave peak in "wind only" conditions seems to result from an over-dissipation in the wind wave frequency range. The wind waves observed in the wind wave tank, especially in "wind only" conditions, are very steep. The saturation limits defined by Ardhuin et al. (2010) and van der Westhuysen (2007) might then be too restrictive for young laboratory wind waves, according to their wave age. Hence, the saturation limit might be more relevant with a definition including a function of wave age. This could allow having a more pronounced overshoot in the spectra and an accurate numerical estimation of the energy levels for both the wind wave peak and the HF tail. This saturation limit is less problematic for wind waves in the presence of longer waves

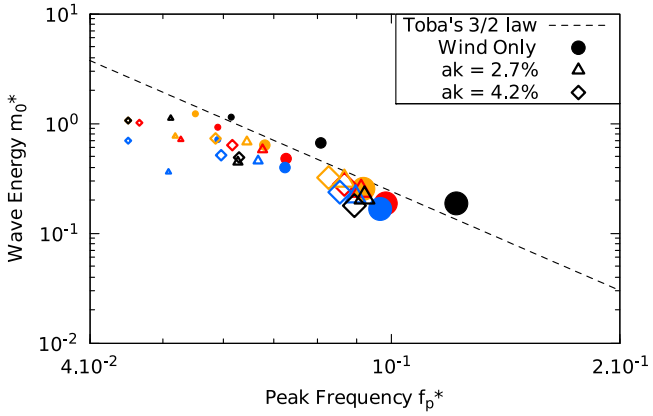

Fig. 5. Variations of the wind waves's dimensionless energy with the dimensionless peak frequency for different reference wind speeds compared to Toba's 3/2 law. The dot size refers to the wind speed (small U_{ref} = 6 m/s; medium U_{ref} = 10 m/s; large U_{ref} = 14 m/s) and the color refers to the sets of source/sink terms. The black points refer to the observations.

since their steepness is reduced due to the background long-waves. The mechanisms at play in this steepness reduction will be further investigated in the following.

5. Hindcast of SHOWEX experiment

5.1. Numerical specifications

The bathymetry for the North Carolina continental shelf was taken from the GEneral Bathymetric Chart of the Oceans (GEBCO) publicly available bathymetry data sets. The different domains are discretized as follows:

- Spatial: irregular mesh with an average resolution of 500 m.
- Temporal: constant time step of 30 s.
- Frequency: 40 frequencies with a logarithmic distribution ($f_n = f_1.q^{n-1}$) over the range [0.04; 0.72] Hz.
- Directional: regular mesh with 36 directions (every 10°).

It was checked that halving the spatial resolution from 500 m to 250 m does not change the simulated spectra, the spatial mesh convergence is thus satisfied.

The wind field is taken from the CFSR time series in open-access in the National Oceanic and Atmospheric Administration (NOAA) website. Fig. 6 gives an overview of the numerical spatial domain colored with the wind velocity (65,000 nodes). It depicts the wind acceleration when the distance to the coast increases. The swell frequency spectra from the measurements at the X6 buoy (offshore) are imposed as boundary condition on the offshore side of the spatial domain. The unstable atmospheric boundary layer is not taken into account in the simulations. These atmospheric conditions would result in a slight wind wave growth amplification (see Ardhuin et al. (2007) for more details). Therefore, this amplification is ignored in our case since the default numerical settings consider a neutral atmospheric boundary layer.

When using Q^{ST4}, it was found that imposing a parametric HF tail was not necessary to obtain a variance density smooth f^{-4} decrease rate. This decrease rate has been largely discussed in the literature (Toba, 1973) and is supported by numerous observations (Kawai et al., 1977). Furthermore, the deactivation of the parametric tail was required to obtain spatially converged results (not shown).

When using $Q^{ST4+GQM}$, neither the parametric HF tail nor the wave growth limiter were activated. These features are commonly used respectively to insure the physical shape of the spectrum at high frequencies and to guarantee the numerical stability of the calculations due to the physical shortcomings of the model parameterizations. Having numerically stable simulations without using these tools is a proof of the physical relevance of the ST4 + GQM parameterization.

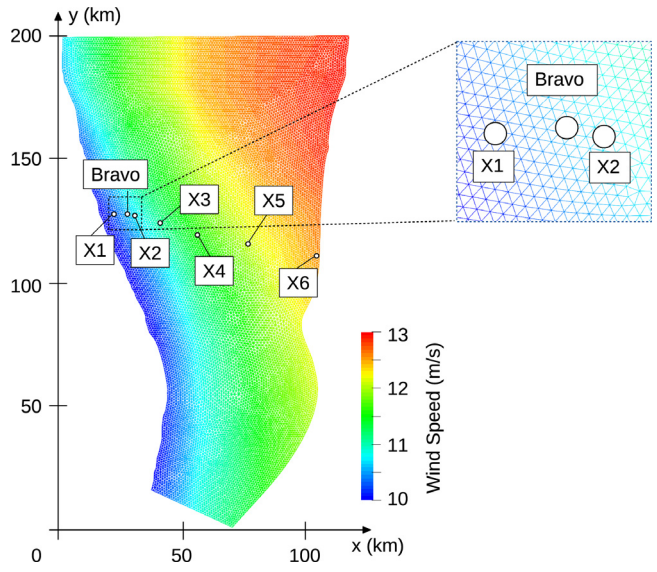

Fig. 6. TOMAWAC's spatial domain showing the wind speed and the irregular mesh adopted for the simulations of the SHOWEX campaign.

5.2. Results

In Section 4, the numerical model has proved to be quite adapted, with a friction velocity forcing, for reproducing the laboratory bimodal sea states. The purpose of our work is to assess the extent at which laboratory observations by Villefer et al. (2021) can be transported at coastal scale. Hence, it is necessary to verify the model's performances for simulating bimodal sea states at coastal scale. This validation step is based on the evaluation of TOMAWAC's performances in reproducing the spatial characteristics of wind wave growth over an opposing background swell within the scope of the SHOWEX campaign.

Fig. 7 depicts the simulated wind wave energy and peak frequency variations with fetch. These variations are compared to the SHOWEX observations and Kahma and Calkoen (1992) law for stable stratification obtained from a collection of laboratory and ocean data.

In the observations, one can distinguish two kinds of gray circles referring to two spectral methods for separating wind waves from swell. The open circles refer to Ardhuin et al. (2007)'s analysis considering the wind-sea energy at frequencies above the first maximum of the directional spread over frequencies. The solid circles refer to a spectral separation method based on JONSWAP-type spectra fitted on the observed bimodal spectra from Villefer et al. (2021). This method is also used to obtain the simulated wind wave energy and peak frequencies. Hence, the model's results are compared to the observations according to the full circles in the following. The vertical distance between solid and empty circles at each fetch, in Fig. 7, depicts the degree of arbitrariness existing between methods for separating swell and wind waves.

In Fig. 7.a, each parameterization reproduces energy variations in agreement with SHOWEX observations and the empirical laws for the energy and the peak frequency. However, the wind wave energy level is systematically overestimated in the simulations especially by VDW at a medium fetch. This systematic overestimation can be explained, to some extent, by the choice of the wind hindcast file. A finer setting of the parameterizations' design parameters, such as Alday et al. (2021) did by modifying the wind input and dissipation parameters for global scale applications, could improve the quality of the estimated energy level. For example, Ardhuin et al. (2007) TEST443 parameterization for ST4 (black triangles in Fig. 7) is in close agreement with the observations (open circles). It should be noted that GQM was activated without changing any dissipation or wind input settings originally calibrated for DIA method. Performing global hindcasts would be necessary to

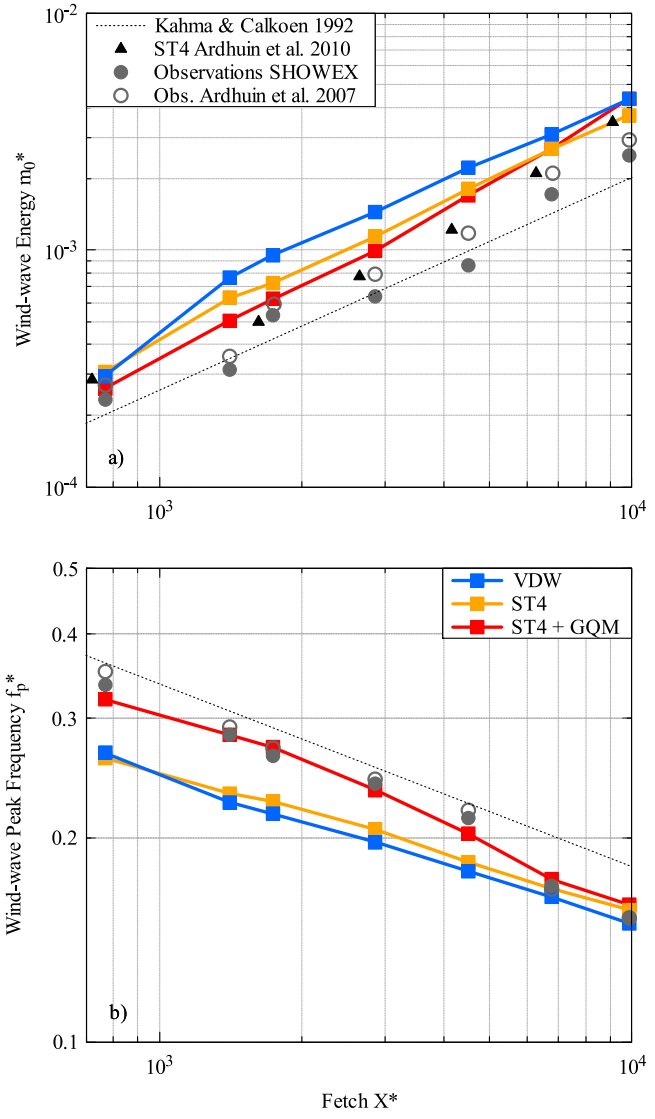

Fig. 7. Variations of the wind wave dimensionless energy (a) and peak frequency (b) with dimensionless fetch (with increasing fetch: X1, Bravo and X2 to X6) compared to Kahma and Calkoen (1992)'s empirical law during SHOWEX campaign on Nov. 3, 1999, 12-17 EST. Color point-lines (blue, orange and red) correspond to simulations with different sets of source/sink terms. Black and gray point-lines refer to the observations.

further improve GQM performances by adopting a finer setting for GQM parameters. Recently, Beyramzadeh and Siadatmousavi (2022) implemented the GQM method in WW3 and performed hindcasts on hurricanes observed in the Gulf of Mexico. Their conclusion, similar to ours, is that a redesign and a recalibration of Q_{in} and Q_{ds} would be necessary to fully benefit from GQM's improvements.

Regarding Fig. 7.b, ST4 + GQM (red lines) clearly outperforms the parameterization using DIA method in reproducing the downshift of the wind wave peak frequency with fetch. The frequency variation depicted by the red curve is in agreement with SHOWEX observations and the empirical law. The differences with parameterizations based on DIA appear at short fetch with an underestimation of the peak frequency. This initial underestimation results in reduced variations that eventually give an accurate peak frequency at longer fetch.

Fig. 8 shows the spatial evolution of frequency spectra at buoys Bravo, X3 and X6 (respectively the 2nd, 4th and last locations relative to increasing fetch in Fig. 7). The features observed in Fig. 7 are encountered again in Fig. 8 with the overestimation of the wind wave

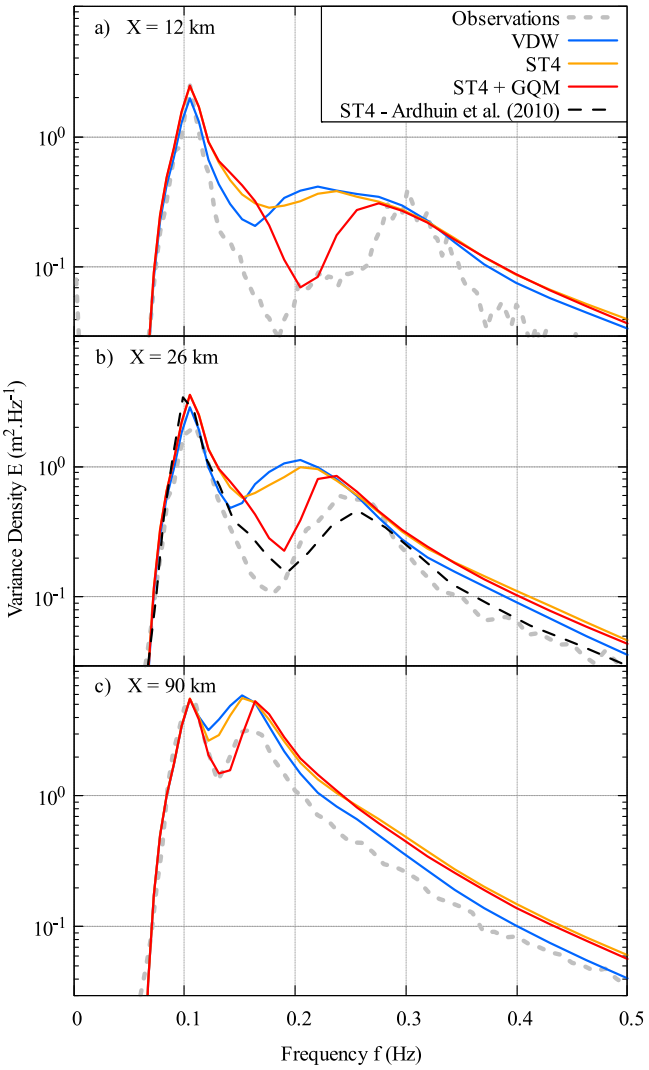

Fig. 8. Spatial evolution of the variance density spectrum with buoys Bravo (X = 12 km), X3 (X = 26 km) and X6 (X = 90 km) during SHOWEX campaign on Nov. 3, 1999, 12-17 EST. Color lines (blue, orange and red) correspond to simulations with different sets of source/sink terms, gray dotted-lines refer to the observations and black dashed-line to Ardhuin et al. (2007) simulation.

energy and the accurate estimation of the wind wave peak frequency by ST4 + GQM. The swell peak is rather well reproduced in the simulations. VDW parameterization shows a stronger dissipation of the swell with fetch resulting from the dissipation term partly based on Komen et al. (1984). In Fig. 8.a and b, the ST4 + GQM simulations (red spectra) overestimate the HF side of the swell peak degrading the agreement with the observations. This overestimation can either result from the 4-wave interactions or from a lack of dissipation of the HF part of the swell in the shoaling process. The overestimation eventually disappears at maximal fetch (Fig. 8.c).

Another proof of ST4 + GQM performances is illustrated by the width of the simulated spectra. While VDW and ST4 parameterizations depict a rather large wind wave peak in Fig. 8.a and b, ST4 + GQM gives a narrower peak which is more representative of the observed spectra.

Fig. 9 shows a set of observed and simulated directional spectra at Bravo location. One should keep in mind that the methods to obtain directional spectra from buoy measurements such as gauge arrays (ASIS) or single-point systems (DDW) only give an estimation of the directional properties. The energy distribution along frequencies and directions can vary between the different methods. Here, the directional spectra from the observations are obtained using the Maximum Likelihood Method (MLM). A classification of methods to analyze directional wave spectra was performed by Benoit et al. (1997).

In Fig. 9, the original directional spectra are multiplied by the squared frequency to highlight the energy of the wind waves. Directional spectra from simulations with and without swell are plotted to assess the extent at which swell impacts the wind wave direction. Looking at the observations in Fig. 9.a, the equilibrium range (clear blue) is slightly deviated from the wind direction towards the alongshore direction. However, the wind wave peak (dark blue–green color) direction is aligned with wind direction.

Using the same SHOWEX event, this deviation has been addressed by Ardhuin et al. (2007) and Zhang et al. (2009). First, by observing the wind wave mean directions, Ardhuin et al. (2007) and Ardhuin et al. (2010) associated this deviation to the slanting fetch properties. They observed a similar but amplified wind wave deviation in their models with a significant bias, compared to SHOWEX observations, towards the alongshore direction. This amplification was even more marked with a saturation-based dissipation term.

Zhang et al. (2009) argued that the slanting fetch has the property to deviate the wind wave peak but not the waves in the equilibrium range. According to them, the waves in the equilibrium range are deviated due to the wind stress angle that can be shifted from the wind direction by the presence of ocean currents.

In the present simulations, no current is taken into account and no shifting of the wave equilibrium range is observed in the corresponding spectra plotted in Fig. 9. The numerically estimated wave equilibrium range has the same direction as the wind in all parameterizations. However, according to VDW and ST4 parameterizations with and without swell, the wind wave peak direction has a bias of about 30° in the alongshore direction. This bias is certainly due to the slanting fetch properties somehow amplified by the numerical model. VDW is the only parameterization showing a clear wind wave energy amplification in the presence of swell. This amplification is another consequence of the use of Komen et al. (1984)'s dissipation term with a background swell.

The differences between DIA method and GQM to take into account the 4-wave interaction in a sea state including wind waves are well illustrated in Fig. 9. According to Fig. 9.d and g, the wind wave peak simulated with ST4 + GQM differs from VDW and ST4 in terms of directional distribution of the wave energy near the wind wave peak. Three peaks can be distinguished. The main peak (i.e. the more energetic in red) follows the alongshore propagation tendency observed in VDW and ST4, while the secondary peak (i.e. yellow) is aligned with the wind direction. Lastly, the third peak is directed offshore. Overall, with the presence of the secondary peak, GQM + ST4 slightly improves the agreement between the numerical model and the observations. Regarding the mutual influences between swell and wind wave peaks, the wave systems do not seem to have significant effects on each other.

In Fig. 10, the frequency spectra, mean directions and directional spreadings simulated with ST4 + QM are compared to the observations at two values of fetch: 26 km and 89 km (buoys X3 and X6, respectively). At buoy X3, the simulated and observed wind wave peak frequencies are identical (Fig. 10.a). However, the distribution of the wind wave energy is slightly shifted towards HFs in the simulation. A similar shift is encountered regarding the mean direction and the directional spread (Fig. 10.b and c). Hence, as observed in Fig. 9, the simulated mean direction is still slightly overestimated in the alongshore direction. In Fig. 10.c, the simulated wind wave directional spreading is overestimated by about 10°.

At buoy X6, the simulated wind wave peak is in rather good agreement with the observations regarding the main direction and the angular spread (Fig. 10.e and f). Yet, the simulated peak frequency is still shifted towards HFs. Compared to the simulations in Figs. 9, 10 proves that the model shows better performances in reproducing the directional properties at a larger fetch, where the influence of the slanting fetch configuration decreases.

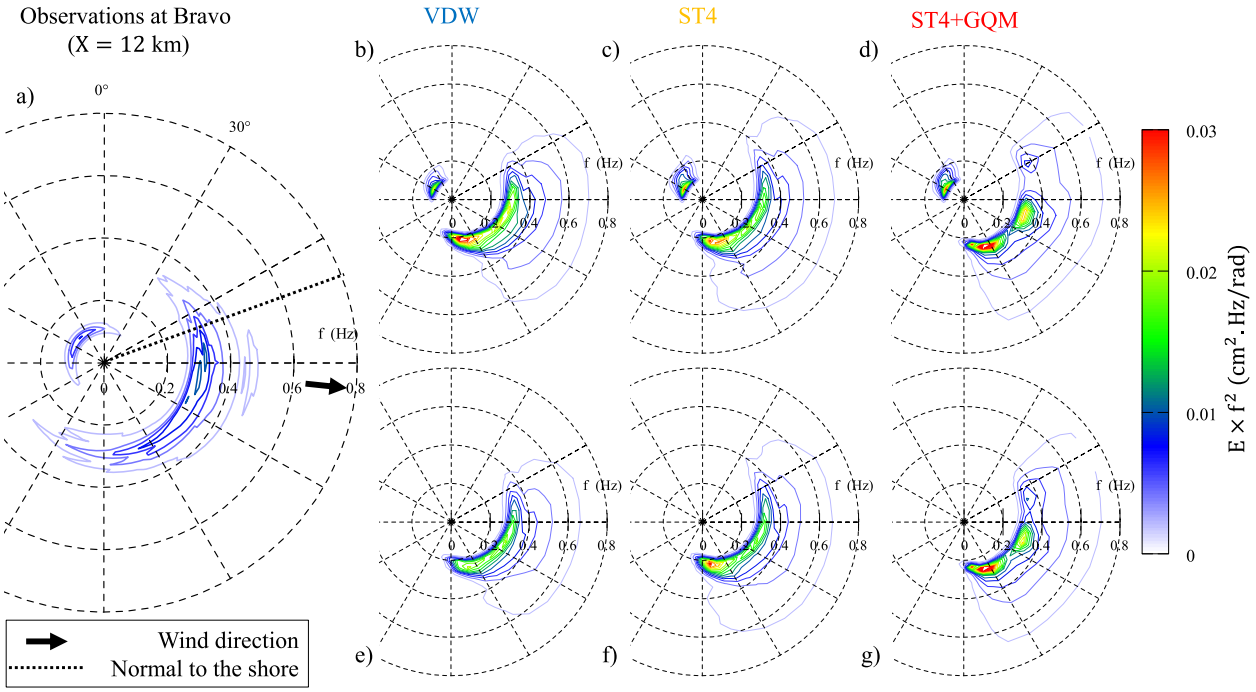

Fig. 9. Directional variance density spectra multiplied by the frequency squared at Bravo (ASIS-type buoy) according to observations using the MLM (a) and to simulations with (b to d) or without (e to g) swell. The normal to the shore is 70° and the mean wind direction is 96°.

The simulations at laboratory and coastal scales prove that the chosen parameterizations are sufficiently accurate to reproduce both laboratory and coastal observations. Among the parameterizations, the aforementioned results showed that ST4 + GQM slightly outperforms simulations with DIA: at laboratory scale in terms of peak frequency variations with fetch and at coastal scale in terms of the directional distribution of the wave energy. ST4 + GQM is used in the next section on a generic case to study the effect of swell on wind wave growth at coastal scale.

6. Application to the study of wind wave growth over swell

6.1. Numerical specifications

A generic mesh was created to study wind wave growth over a background following swell. The maximal fetch for this study was set to 60 km. The mesh resolution is 500 m. The selected generic atmospheric conditions are in such a way that a wind at a velocity $U_{10} = 12$ m/s is blowing over a swell (JONSWAP-type) with a 10 s peak period propagating in the wind direction. Simulations were run with six swell energy levels ranging from no swell to a swell with a significant wave height $H_{m0} = 2$ m. The swell energy levels are identified in Figs. 11 and 12 by swell energy percentages (i.e. 0 to 100% corresponding to 0 to 2 m wave height ; for instance, 40% is equivalent to a swell with $H_{m_0} = \sqrt{0.4} * 2 = 1.26$ m).

Two test cases were selected. In both cases, the ST4 + GQM parameterization is used and the simulations are run with the six different swell magnitudes. The purpose of the first case is to let the wave model handle the whole wind wave generation process and to observe the final results when the sea state reaches a stationary state. For this first case, only the swell, given the aforementioned percentage, is present in the initial condition of the simulations. Fig. 11 shows the corresponding stationary spectra. The second test case, inspired by Masson (1993) study, aims at observing the source term balance for specific sea states consisting in the addition of two JONSWAP spectra. As illustrated in Fig. 12.a, one is the swell system with $f_p = 0.1$ Hz and six different energy levels and the other one represents a wind wave system with $f_p = 0.2$ Hz (5 s peak period) and $H_{m0} = 1$ m. In Fig. 12.a, the wind wave energy levels are slightly affected by swell energy. This is due to the addition of the energy in the HF tail of the JONSWAP swell spectrum. Considering $Q_{\text{in}} + Q_{\text{ds}}$ and Q_{nl}, the source term balance is calculated and given in Fig. 12.b and c.

6.2. Results

As mentioned above, the wind wave modifications in the presence of swell are difficult to observe in the ocean and in coastal areas. This is partly due to the complex notion of fetch when dealing with vast areas of water and winds varying both in space and in time. Here, we suggest using a numerical model to overcome the problem. Fig. 11 proves that, given the parameterizations and hypotheses on which our simulations are based with the use of TOMAWAC, the wind wave generation is largely modified with a background swell.

Given the constant wind speed (U_{10}), the only parameter changing between the different simulations (i.e. different colors) in Fig. 11 is the swell height. The downshift of the wind wave peak frequency with increasing swell height is clear with the wind wave peak frequency varying from 0.2 Hz to almost 0.15 Hz equivalent to a variation from 5 to 6.7 s in terms of peak period. This downshift observed in Fig. 11 is in agreement with the downshift observed during the laboratory experiments (Fig. 1).

In order to further analyze the physical processes leading to the downshift, the source terms involved in TOMAWAC simulations are investigated in Fig. 12. This separation of the physical processes is inspired from Masson (1993) study in which the nonlinear coupling between swell and wind waves was examined. Here, the influence of the balance between the wind energy input and the whitecapping dissipation is studied in addition to the 4-wave interactions term.

According to Fig. 12.b, the balance between Q_{in} and Q_{ds} is positive: wave generation prevails over wave dissipation so wave components are only growing. Hence, at the stage considered in Fig. 12, the wave spectra did not reach an equilibrium state. The observation of this duration-limited stage is necessary to identify the processes leading to the downshift. In Fig. 12.b, the most striking effect of the swell energy

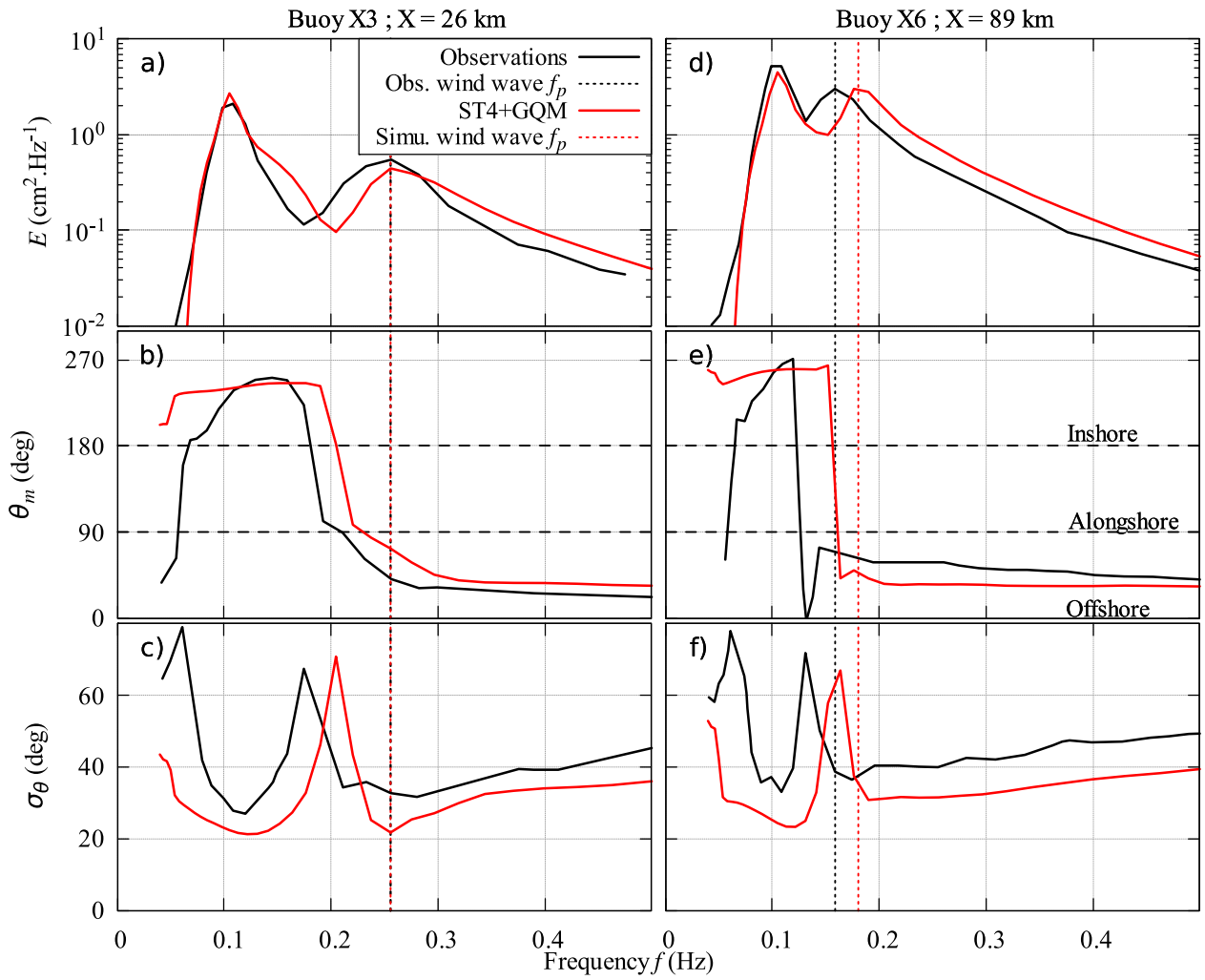

Fig. 10. Simulated (red lines) and observed (black lines) (a,d) frequency spectra, and both as a function of frequency, (b,e) mean directions and (c,f) directional spreadings on 3 Nov. 1999 (averages over the 12:00–17:00 EST time interval) at two values of fetch: 26 km (on the left) and 89 km (on the right). Only the simulation using ST4 + GQM set is displayed. The red and black vertical dotted lines correspond to the simulated and observed (resp.) wind wave peak frequencies.

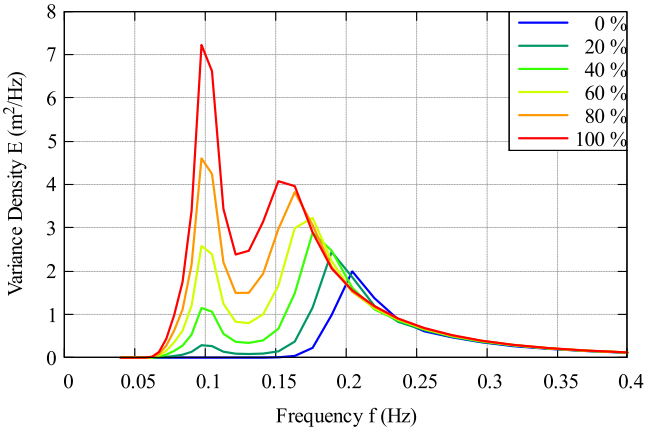

Fig. 11. Downshift of the wind wave's variance density spectra in the presence of swell using TOMAWAC at a fetch 50 km. The swell is characterized by different energy levels identified by percentages: 0% and 100% respectively relate to no swell and to a 2 m high swell (H_{m0}).

on wind wave growth is the large wind wave generation on the HF side of the swell peak. A significant amount of energy is added to the wave system in the frequency range between the swell and the wind wave peaks. Such wave generation on the low frequency part of the wind wave peak facilitates the wind wave frequency downshift. This observation is in agreement with Villefer et al. (2021) hypothesis. According the them, the energy continuum brought by the swell HF tail would initiate wind wave growth at a lower frequency than in absence of swell.

Fig. 12.c recalls (Masson, 1993) study on nonlinear coupling between swell and wind waves. As said above, according to this latter reference, 4-wave interactions are involved in the wind wave evolution when the ratio of swell to wind wave frequency is greater than 0.6. In our case, this ratio is 0.5. In Fig. 12.c, Q_{nl} shows slight variations accounting for the slight differences in wind wave energy levels (see Fig. 12.a). Apart from these variations, the swell does not seem to have a significant effect on the 4-wave interactions term that could have a notable effect on wind wave growth. This latter assertion is in agreement with Masson's ratio.

The present analysis could be completed by studying the magnitude of the downshift as a function of the spectral width of the swell peak. It comes from the present analysis that the HF tail of the swell peak artificially increases the fetch available for wind wave growth by initiating wave generation at a lower frequency than without swell. However, in many cases, swell spectral peaks do not carry much energy in the HF range. Given the latter analysis, the observed downshift is therefore expected to be reduced with a sharper and narrower swell peak. Hence, further analysis could be performed by testing different

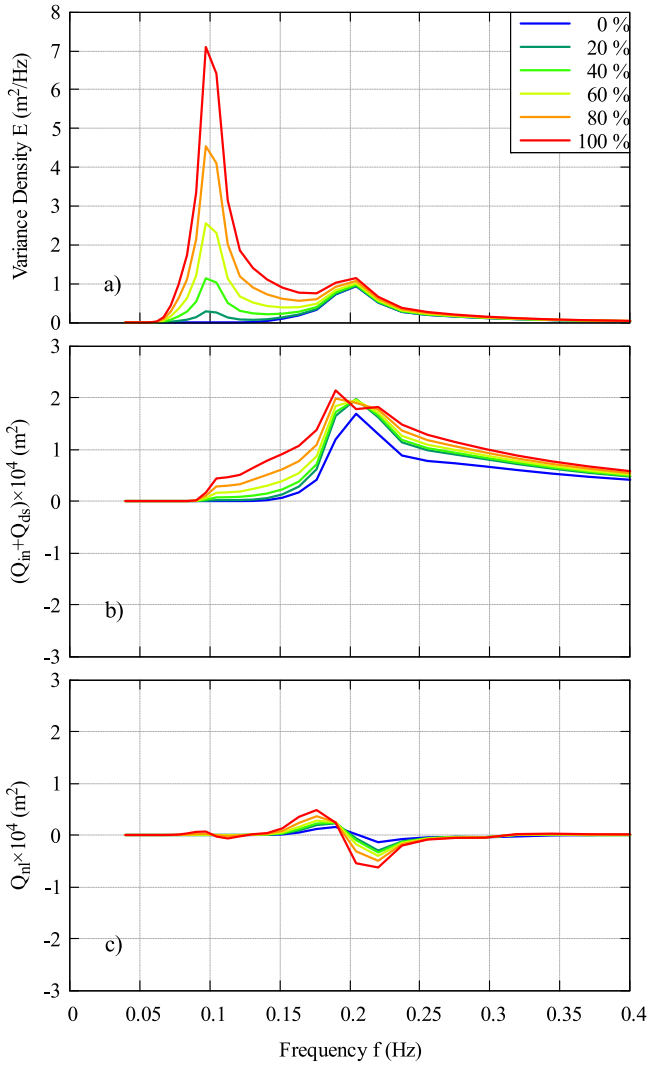

Fig. 12. Bimodal wave spectra with different swell intensity (a) with the associated $Q_{in} + Q_{ds}$ balance (b) and non-linear transfer Q_{nl} (c).

shapes for the swell peak with a narrow Gaussian shape, for instance. This is left for future work.

Overall, studying the influence of swell on wind wave generation based on the use of a spectral wave model with a generic domain enables to gain insights on the physical processes at play in the wind wave growth process for complex sea state conditions. However, this insight may be biased due to the limitations and the large extent of empiricism involved in the physical processes modeled in such numerical models (see e.g. Cavaleri et al. (2007)). Although the general shape of the wave spectrum has been reproduced to some extent by the numerical model at laboratory and coastal scales, the source and sink terms combination is not validated. There is a multitude of combinations between generation and dissipation terms that might lead to the observed spectra. Yet, the gap between the understanding of the physical processes and their mathematical formulations as source and sink terms in 3G wave models is constantly decreasing.

The present analysis, involving wind wave tank experiments and numerical simulations, is still rather exploratory and could be continued to assess the effect of several physical parameters on wind wave growth in more diverse configurations. Parameters such as the wind direction relative to the swell direction, the water depth or the atmospheric stability could be investigated, among others.

7. Extension of the results to real ocean waves

A downshift of the wind wave peak frequency was observed in Marseilles' wind wave tunnel when long paddle-waves were added into the wave system (Villefer et al., 2021). To which extent these laboratory observations can be upscaled at coastal scale with swell instead of paddle-waves? This is not an easy question since the long paddle-waves generated in wind wave tunnels have a wave age radically smaller than typical ocean swell. In the present paper, the method chosen to address the question is based on the use of a 3G spectral wave model. The initial hypothesis is that if the numerical model can faithfully reproduce the laboratory experiments (i.e the frequency downshift) and the evolution of a bimodal sea states (i.e. combining wind waves and swell) at a coastal scale, it can be used to upscale the laboratory experiment to the coastal scale. And by decomposing the physical processes at play when wind waves grow, the model can help to identify the physical processes responsible for the downshift.

The first stage of our methodology was to evaluate TOMAWAC performances in reproducing bimodal sea states at laboratory and coastal scales. Amongst the different parameterizations, the combination ST4 + GQM gives, on average, the best agreement between simulations and observations. Overall, ST4 + GQM shows a rather faithful reproduction of the observations both in terms of wave energy and peak frequency variations with fetch. Nevertheless, there are two main limitations of the model:

- at laboratory scale, the model largely underestimates the wind wave peak energy in wind only conditions (i.e. without paddle-waves),
- at coastal scale, in the presence of slanting fetch conditions of the selected event (SHOWEX campaign), the model succeeds only partially in simulating the directional distribution of the wind wave energy.

Yet, one interesting feature is the numerical simulation of a downshift similar to the experiments at laboratory scale, to a lesser extent though.

The second stage of our methodology consisted in creating a generic coastal domain to upscale the laboratory experiments at coastal scale. The first test case (Fig. 11) reveals a marked wind wave peak frequency downshift, increasing with swell intensity. According to the simulations, the wind wave peak period can be shifted by more than 1 s when a background swell is present. This wave period shift would have significant effects on the design of breakwaters or offshore structures, for instance. In a second test case (Fig. 12), we took advantage of the separation of the physical processes (i.e. Q_{in}, Q_{ds} and Q_{nl}) to identify the source and sink terms responsible for the spectral downshift. The wind input term is the best candidate given the wave generation happening on the low frequency part of the wind wave peak in the presence of swell. This wind wave generation at frequencies lower than without swell appears to be due to the continuum of energy brought by the swell peak in the HF range.

The methodology described in the present study is essentially based on the wave model reliability in modeling the physical processes at play when wind waves grow. This validity was evaluated to a large extent by performing comparisons between the numerical model results and wave observations. Such a verification makes our methodology more consistent, but the results must be appreciated in light of the validation stage we performed.

8. Conclusion

The performances of a 3G wave model were assessed for the simulation of bimodal sea state conditions at laboratory and coastal scales. Three sets of parameterizations for the source and sink terms were tested and compared with the observations at both scales. The similarity between the different sets lies in the modeling of the dissipation by whitecapping using a saturation based model. The latter choice results from the limitations of Komen et al. (1984) dissipation model in bimodal sea state conditions highlighted in several references (e.g. Ardhuin et al., 2007).

The ST4 + GQM combination, recently and originally developed in TOMAWAC, uses a highly accurate method (GQM) to compute the nonlinear 4-wave interactions (Benoit, 2005; Gagnaire-Renou et al., 2010). Within this set, GQM is combined with the recent and largely adopted ST4 parameterization for the whitecapping dissipation sink term (Ardhuin et al., 2010). Compared to the other sets based on the DIA method, ST4 + GQM simulations are roughly 50 times longer than the other sets due to the CPU time to compute Q_{nl} with GQM.

Overall, all the sets of parameterizations showed good performances for the reproduction of the frequency spectra by comparison with the observations at both scales. The ST4 + GQM combination, albeit computationally demanding, showed two interesting facets:

- at laboratory scale, it differentiates from the other sets with a very accurate reproduction of the wind wave peak frequency variations with fetch,
- at coastal scale, it is the set showing the best agreement in terms of directional properties by comparison with the observations.

In addition to these two facets, simulations with ST4 + GQM can be run without imposing any diagnostic HF tail and without using any wave growth limiter. Lastly, the ST4 + GQM set was used to investigate the relevance of a physical phenomenon observed at laboratory scale, within a bimodal sea state combining two wind wave systems, at coastal scale within a bimodal sea state combining swell and wind waves.

To improve the results of the present study, it would be necessary to remove the friction velocity forcing, adopted for the simulations at laboratory scale. Recent studies aimed to improve the calculation of the friction velocity by further including the effects of nonlinearity with Janssen and Bidlot (2021) revision of Janssen (1991) source term or with the use of a wave boundary layer model as in Du et al. (2017). To further improve the directional properties of the simulated spectra, Romero (2019) proposed an anisotropic parameterization of the dissipation by whitecapping showing promising directional properties.

The use of 3G spectral wave models at laboratory scale could permit to further validate the different parameterizations for the source and sink terms in idealized conditions. Lastly, the simulations on a generic coastal domain could be continued to investigate wind wave growth with a background swell considering several aspects such as the relative angle between swell and wind direction, the presence of a variable depth, the directional spread of the swell system, etc.

CRediT authorship contribution statement

Antoine Villefer: Methodology, Investigation, Writing – original draft. **Michel Benoit:** Supervision, Conceptualization, Writing – review and editing. **Damien Violeau:** Supervision, Conceptualization, Writing – review and editing. **Maria Teles:** Supervision, Numerical investigation, Writing – review and editing.

Declaration of competing interest

The authors declare that they have no known competing financial interests or personal relationships that could have appeared to influence the work reported in this paper.

Data availability

Data will be made available on request.

Acknowledgments

Antoine Villefer acknowledges the financial support of his PhD research program provided by the French ANRT (Association Nationale de la Recherche et de la Technologie) with CIFRE grant number 2019-1257. The authors thank Dr. Fabrice Ardhuin (LOPS, UMR 6523, Brest, France) and Pr. William Drennan (RSMAS, Miami, FL, USA) for providing the SHOWEX data, and Dr. Hubert Branger (IRPHE, UMR 7342, Marseilles, France) and Dr. Jeffrey Harris (ENPC/LHSV, Chatou, France) for many fruitful discussions.

References

Alday, M., Accensi, M., Ardhuin, F., Dodet, G., 2021. A global wave parameter database for geophysical applications. Part 3: improved forcing and spectral resolution. Ocean Model. 166, 101848.

Alves, J.-H.G.M., Banner, M., 2003. Performance of a saturation-based dissipation-rate source term in modeling the fetch-limited evolution of wind waves. J. Phys. Oceanogr. 33, 1274–1298.

Ardhuin, F., Herbers, T., Jessen, P., O'Reilly, W., 2003a. Swell transformation across the continental shelf. Part ii: validation of a spectral energy balance equation. J. Phys. Oceanogr. 33, 1940–1953.

Ardhuin, F., Herbers, T., O'Reilly, W., Jessen, P., 2003b. Swell transformation across the continental shelf. Part i: attenuation and directional broadening. J. Phys. Oceanogr. 33, 1921–1939.

Ardhuin, F., Herbers, T., van Vledder, G., Watts, K., Jensen, R., Graber, H., 2007. Swell and slanting-fetch effects on wind wave growth. J. Phys. Oceanogr. 37, 908–931.

Ardhuin, F., Rogers, E., Babanin, A., Filipot, J.-F., Magne, R., Roland, A., Van Der Westhuysen, A.J., Queffeulou, P., Lefevre, J.-M., Aouf, L., Collard, F., 2010. Semiempirical dissipation source functions for ocean waves. Part i: definition, calibration, and validation. J. Phys. Oceanogr. 40, 1917–1941.

Barnett, T.P., Sutherland, A.J., 1968. A note on an overshoot effect in wind-generated waves. J. Geophys. Res. 73 (22), 6879–6885.

Benoit, M., 2005. Evaluation of methods to compute the non-linear quadruplets interactions for deep-water wave spectra.. In: Proceedings of the Fifth International Symposium on Ocean Waves Measurement and Analysis, Madrid (ESP), 3–7 July 2005, Waves 2005. American Society of Civil Engineering, pp. 1–10.

Benoit, M., Frigaard, P., Schäffer, H., 1997. Analyzing multidirectional wave spectra: a tentative classification of available methods. In: Proceedings of the 1997 IAHR Conference, San Francisco (CA, USA). pp. 131–158.

Benoit, M., Marcos, F., Becq, F., 1996. Development of a third generation shallow-water wave model with unstructured spatial meshing. In: Proceedings of the 25th International Conference on Coastal Engineering (ICCE'1996), Orlando (FL, USA). American Society of Civil Engineers, pp. 465–478.

Beyramzadeh, M., Siadatmousavi, S.M., 2022. Skill assessment of different quadruplet wave-wave interaction formulations in the WAVEWATCH-III model with application to the Gulf of Mexico. Appl. Ocean Res. 127, 103316. http://dx.doi.org/10.1016/j.apor.2022.103316.

Bidlot, J., Janssen, P.A.E.M., Abdalla, S., 2007. A Revised Formulation of Ocean Wave Dissipation and its Model Impact. Technical Report. ECMWF Tech. Rep. Memo. 509, Reading, United Kingdom, p. 27.

Booij, N., Holthuijsen, L.H., Haagsma, I.J., 2001. The effect of swell on the generation and dissipation of wind sea. In: 4th International Symposium on Ocean Wave Measurement and Analysis, San Francisco. USA, pp. 501–506.

Booij, N., Ris, R.C., Holthuijsen, L.H., 1999. A third-generation wave model for coastal regions: 1. Model description and validation. J. Geophys. Res.: Oceans 104 (C4), 7649–7666.

Cavaleri, L., Alves, J.-H.G.M., Ardhuin, F., Babanin, A.V., Banner, M., Belibassakis, K.A., Benoit, M., Donelan, M.A., Groeneweg, J., Herbers, T.H.C., Hwang, P.A., Janssen, P.A.E.M., Janssen, T., Lavrenov, I.V., Magne, R., Monbaliu, J., Onorato, M., Polnikov, V., Resio, D., Rogers, W.E., Sheremet, A., McKee Smith, J., Tolman, H.L., van Vledder, G., Wolf, J., Young, I., 2007. Wave modeling - the state of the art. Prog. Oceanogr. 74, 603–674.

Cavaleri, L., Malanotte Rizzoli, P., 1981. Wind wave prediction in shallow water: theory and applications. J. Geophys. Res.: Oceans 86 (C11), 10961–10973.

Chen, G., Belcher, S.E., 2000. Effects of long waves on wind-generated waves. J. Phys. Oceanogr. 30, 2246–2256.

Donelan, M.A., 1987. The effect of swell on the growth of wind waves. In: Johns Hopkins APL Technical Digest. pp. 18–23.

Donelan, M.A., Drennan, W.M., Katsaros, K., 1997. The air-sea momentum flux in conditions of wind sea and swell. J. Phys. Oceanogr. 27, 2087–2099.

Du, J., Bolaños, R., Guo Larsén, X., 2017. The use of a wave boundary layer model in SWAN. J. Geophys. Res.: Oceans 122 (1), 42–62.

Gagnaire-Renou, E., Benoit, M., Forget, P., 2010. Ocean wave spectrum properties as derived from quasi-exact computations of nonlinear wave-wave interactions. J. Geophys. Res.: Oceans 115, C12058.

Graber, H.C., Terray, E.A., Donelan, M.A., Drennan, W.M., Leer, J.C.V., Peters, D.B., 2000. ASIS—A new air–sea interaction spar buoy: design and performance at sea. J. Atmos. Ocean. Technol. 17 (5), 708–720.

Hasselmann, K., 1962. On the non-linear energy transfer in a gravity-wave spectrum. Part 1. General theory. J. Fluid Mech. 12 (4), 481–500.

Hasselmann, K., 1974. On the spectral dissipation of ocean waves due to white capping. Bound.-Lay. Meteorol. 6, 107–127.

Holthuijsen, L.H., Ris, R.C., Booij, N., Cecchi, E., 2000. Swell and whitecapping - a numerical experiment. In: Proceedings of the 27th International Conference on Coastal Engineering (ICCE'2000), Sydney. AUS, ASCE, pp. 346–354.

Hwang, P.A., García-Nava, H., Ocampo-Torres, F.J., 2011. Observations of wind wave development in mixed seas and unsteady wind forcing. J. Phys. Oceanogr. 41, 2343–2362.

Janssen, P.A.E.M., 1991. Quasi-linear theory of wind-wave generation applied to wave forecasting. J. Phys. Oceanogr. 21, 1631–1642.

Janssen, P.A.E.M., 2004. The Interaction of Ocean Waves and Wind. Cambridge University Press.

Janssen, P.A.E.M., Bidlot, J.-R., 2021. On the Consequences of Nonlinearity and Gravity-Capillary Waves on Wind-Wave Interaction. Technical Report. ECMWF Tech. Rep. Memo. 882, Reading, United Kingdom, p. 40.

Kahma, K.K., Calkoen, C.J., 1992. Reconciling discrepancies in the observed growth of wind-generated waves. J. Phys. Oceanogr. 22 (12), 1389–1405.

Kawai, S., Okada, K., Toba, Y., 1977. Field data support of three-seconds power law and $gu * \sigma^{-4}$-spectral form for growing wind waves. J. Oceanogr. Soc. Japan 33, 137–150.

Kitaigorodskii, S., 1961. Application of the theory of similarity to the analysis of wind generated wave motion as a stochastic process. Izv. Akad. Nauk SSSR Ser. Geofiz. 1, 105–117.

Komen, G.J., Hasselmann, S., Hasselmann, K., 1984. On the existence of a fully developed wind-sea spectrum. J. Phys. Oceanogr. 14, 1271–1285.

Lavrenov, I.V., 2001. Effect of wind wave parameter fluctuation on the nonlinear spectrum evolution. J. Phys. Oceanogr. 31 (4), 861–873.

Mason, T., Bradbury, A., Poate, T., Newman, R., 2008. Nearshore wave climate of the English Channel evidence for bimodal seas. In: Proceedings of the 31st International Conference on Coastal Engineering (ICCE'2008), Hamburg. DEU, World Scientific, pp. 605–616. http://dx.doi.org/10.1142/9789814277426_0051.

Masson, D., 1993. On the nonlinear coupling between swell and wind waves. J. Phys. Oceanogr. 23, 1249–1258.

Mitsuyasu, H., 1966. Interactions between water waves and wind (1). Rep. Inst. Appl. Mech. Kyushu Univ. 14, 67–88.

Monin, A.S., Obukhov, A.M., 1954. Basic laws of turbulent mixing in the surface layer of the atmosphere. Tr. Akad. Nauk SSSR Geophiz. Inst. 24, 163–187.

Pettersson, H., Kahma, K.K., Tuomi, L., 2010. Wave directions in a narrow bay. J. Phys. Oceanogr. 40 (1), 155–169.

Phillips, O.M., Banner, M.L., 1974. Wave breaking in the presence of wind drift and swell. J. Fluid Mech. 66, 625–640.

Romero, L., 2019. Distribution of surface wave breaking fronts. Geophys. Res. Lett. 46 (17 - 18), 10463–10474. http://dx.doi.org/10.1029/2019GL083408.

Shemer, L., 2019. On evolution of young wind waves in time and space. Atmosphere 10 (9), 562.

The WAVEWATCH III (R) Development Group (WW3DG), 2019. User Manual and System Documentation of WAVEWATCH III (R) version 6.07. Technical Report. Tech. Note 333, NOAA/NWS/NCEP/MMAB, College Park, MD, USA, p. 465, + Appendices.

Thompson, D.A., Karunarathna, H., Reeve, D.E., 2018. An analysis of swell and bimodality around the south and south-west coastline of England. Nat. Hazards Earth Syst. Sci. Discuss. 1–28. http://dx.doi.org/10.5194/nhess-2018-117, [preprint].

Toba, Y., 1973. Local balance in the air-sea boundary processes. III On the spectrum of wind waves. J. Oceanogr. Soc. Japan 29, 209–220.

Toba, Y., 1997. The 3/2-power law for ocean wind waves and its applications. In: Advances in Coastal and Ocean Engineering, Vol. 3. World Scientific, pp. 31–65.

Tolman, H.L., Chalikov, D., 1996. Source terms in a third-generation wind wave model.. J. Phys. Oceanogr. 26, 2497–2518.

van der Westhuysen, A.J., 2007. Advances in the Spectral Modelling of Wind Waves in the Nearshore (Ph.D. thesis). Delft University of Technology, Delft, The Netherlands.

van der Westhuysen, A.J., Zijlema, M., Battjes, J.A., 2007. Nonlinear saturation-based whitecapping dissipation in SWAN for deep and shallow water. Coast. Eng. 54 (2), 151–170. http://dx.doi.org/10.1016/j.coastaleng.2006.08.006.

Villefer, A., Benoit, M., Violeau, D., Luneau, C., Branger, H., 2021. Influence of following, regular, and irregular long waves on wind-wave growth with fetch: an experimental study. J. Phys. Oceanogr. 51 (11), 3435–3448.

Vincent, C.L., Thomson, J., Graber, H.C., Collins III, C.O., 2019. Impact of swell on the wind-sea and resulting modulation of stress. Prog. Oceanogr. 178, 102164.

Zakharov, V.E., 1968. Stability of periodic waves of finite amplitude on the surface of a deep fluid. J. Appl. Mech. Tech. Phys. 9, 190–194.

Zhang, F.W., Drennan, W.M., Haus, B.K., Graber, H.C., 2009. On wind-wave-current interactions during the shoaling waves experiment. J. Geophys. Res.: Oceans 114, C1018.